



HAL
open science

From photons to electrons: a complete 3D simulation flow for CMOS image sensor

Crocherie Axel, Boulenc Pierre, Jérôme Vaillant, Hirigoyen Flavien, Hérault
Didier, Tavernier Clément

► To cite this version:

Crocherie Axel, Boulenc Pierre, Jérôme Vaillant, Hirigoyen Flavien, Hérault Didier, et al.. From photons to electrons: a complete 3D simulation flow for CMOS image sensor. IISW 2009 - IEEE 2009 International Image Sensor Workshop, IEEE, Jun 2009, Bergen, Norway. pp.P15. hal-04235628

HAL Id: hal-04235628

<https://hal.science/hal-04235628>

Submitted on 10 Oct 2023

HAL is a multi-disciplinary open access archive for the deposit and dissemination of scientific research documents, whether they are published or not. The documents may come from teaching and research institutions in France or abroad, or from public or private research centers.

L'archive ouverte pluridisciplinaire **HAL**, est destinée au dépôt et à la diffusion de documents scientifiques de niveau recherche, publiés ou non, émanant des établissements d'enseignement et de recherche français ou étrangers, des laboratoires publics ou privés.

From photons to electrons: a complete 3D simulation flow for CMOS image sensor

Axel Crocherie, Pierre Boulenc, Jérôme Vaillant, Flavien Hirigoyen, Didier Hérault, Clément Tavernier
STMicroelectronics, 850 rue Jean Monnet, 38920 Crolles, France

Abstract — This paper presents the 3-Dimensional simulation flow we have developed at STMicroelectronics for CMOS Image Sensor modeling. In this purpose, we coupled Optical simulations with TCAD process and device simulations to combine both approaches benefits. After describing the electromagnetic simulation of the light propagation inside the pixel structure and the framework for the simulation of the photo-generated electrons collection by the photodiodes, a comparison is made between our coupled Optical/TCAD simulations results and real Image Sensors optical measurements. The accuracy and predictability of this methodology is demonstrated on various 1.75 μm pitch pixels.

Index Terms—Image sensors, Simulation, FDTD methods, Optical propagation, Semiconductor devices modeling, TCAD.

I. INTRODUCTION

As pixel size shrinks in CMOS image sensors markets, the crosstalk effects become more and more critical. They can be divided in two components: the optical crosstalk due to the light propagation inside the pixel itself (including color filters transmission curves), and the electrical crosstalk related to the minority carrier diffusion and collection efficiency inside the substrate. Since these crosstalks are strongly interdependent, coupled Optical/TCAD simulations are mandatory to accurately reproduce this interaction and thus real pixel performances.

The next section deals with the methodology we used: on one hand for the Optical simulation tool, and on the other hand for the Electrical simulation tool. The third section presents the whole simulation flow calibration and the comparison between obtained results and experimental measurements.

II. METHODOLOGY

A. Optical part

1) FDTD

For small pixels that are used nowadays in CMOS image sensors, diffraction effects can substantially affect light propagation and photon collection. Thus, ray-tracing description is not accurate anymore [1] and we must use a more fundamental description to simulate these optical effects. We chose to adopt an electromagnetic simulation tool based on Finite Difference Time Domain (FDTD) [2,3], available from Lumerical Solutions [4], to describe light propagation and photon collection inside the pixels while correctly simulating diffraction effects.

FDTD is a fully vectorial method that gives both time-domain and frequency domain information by exploiting Fourier Transforms, i.e. when a broadband pulse is used as the source, the response of the system over a wide range of wavelengths could be obtained in a single simulation. Thus, this method is well adapted to our topic as we will be

interested in a frequency averaging around the wavelength of interest (450nm, 532nm, and 633nm). We will discuss later about this subject.

2) Pixel modeling

Lumerical software allows us to import the GDS layouts created by designers to generate a 3-Dimensional representation of the pixels. Besides, specific shape of microlenses could also be imported in the software from the AFM data. This allows a complete and real modeling of the pixels as we could see on Fig. 1 below for a 1.75 μm pixel.

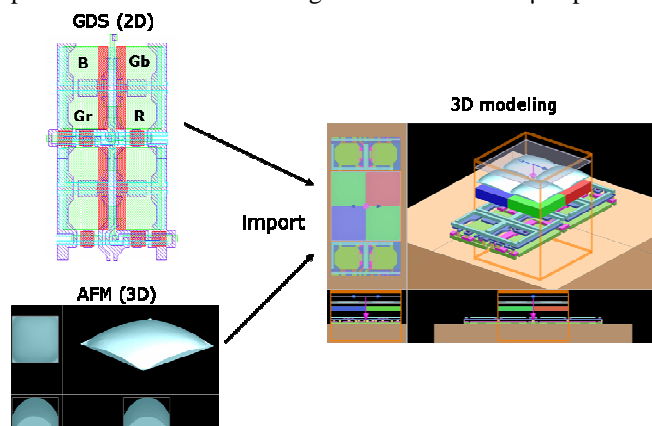


Fig. 1 3D modeling of pixels with the optical simulation tool

In the simulation, we are interested in the response of the blue, the green, and the red pixels of the structure. As the layout is periodic for the four pixels of the Bayer pattern, we will only simulate these pixels with periodic boundary conditions at the four lateral sides of the structure. Besides, absorbing boundary conditions are used at the top and the bottom of the structure to avoid unwanted reflections.

Materials used, like oxides, nitrides, silicon, color filters, are based on STMicroelectronics experimental database. Refractive indexes of these materials are parameterized in Lumerical tool to rigorously simulate their dispersion on the whole visible spectrum of the simulation [4, 5]. Finally, metal for the interconnections are considered as perfect conductors (in this way, any wave reaching the metal line is reflected with the same incident angle and without any attenuation).

3) Accuracy of simulation: mesh step

The mesh step affects the accuracy of the simulation: a smaller mesh step will give more accurate results but requires more resources. One defines a parameter N_λ that represents the number of mesh cells per wavelength as shown by:

$$N_\lambda = \frac{\lambda}{\Delta x \cdot n} \quad (1)$$

with Δx the mesh step along one direction of the grid, λ the smallest wavelength of the simulation source, and n the highest

refractive index of the simulation structure. The mesh step has been fixed to $N_{\lambda}=10$ here with the adaptive grid, a good trade-off between mesh accuracy and resources requirement for 3D simulations [5].

4) Source modeling

The source development is a key part of this methodology. We need a source that reproduces a product-like illumination, keeping reasonable computation time and memory. Regarding scaling problems between the objective-lens (several millimeters) and the pixels (several micrometers), we chose to adopt a local approach by simulating a group of pixels receiving the same uniform illumination from the exit pupil of the objective-lens (see Fig. 2). We have demonstrated in a previous paper [6] that this kind of diffuse-like source could be represented by the incoherent sum of angularly uniformly distributed plane waves with incidence angles limited by the f-number of the objective-lens.

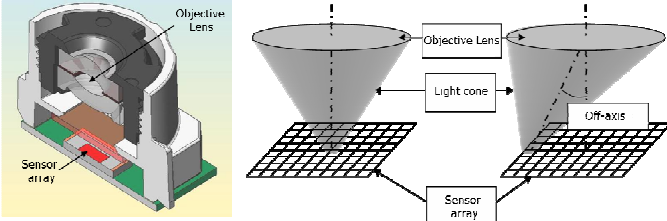


Fig. 2 Light shape in the case of a uniform pixel illumination provided by an objective-lens

Interference inside the sensor back-end-of-line (BEOL) causes oscillations on the transmission spectrum. In order to smooth them but also to take into account the dispersion that exists in process for layers' thicknesses, optical simulations are made on a narrowband spectrum ($\pm 10\text{nm}$ with a 1nm sample step) around the wavelengths of interest. Then results are incoherently averaged.

Finally, we have to set the power of the source. As we make here an electro-optical coupling tool, we must simulate a realistic number of electrons in the silicon, i.e. a realistic number of photons at the input of the optical simulator. We consider here a pixel of $1.75\mu\text{m}$ pitch with a full well capacity of 9000 electrons [7]. At mid-saturation, with a quantum efficiency around 45%, this leads to roughly $N_{\text{photons}}=10,000$ photons at the source input. Then, we could calculate the source power I_{λ} (in $\text{W}\cdot\text{m}^{-2}$) using the following equation:

$$I_{\lambda} = \frac{N_{\text{photons}} \cdot h\nu}{t_{\text{int}} \cdot A_{\text{pixel}}} \quad (2)$$

with $h\nu$ the photon energy, t_{int} the integration time (equal to 66.7ms , i.e. 15 frames/second), and A_{pixel} the area of the pixel.

5) Optical Generation

The information we want to extract from the optical simulations is the Optical Generation, i.e. the photogenerating rate of electron/hole pairs in the silicon in $\text{m}^{-3}\cdot\text{s}^{-1}$, given by:

$$G_{\text{opt}} = \frac{-\text{Re}(\vec{\nabla} \cdot \vec{P})}{h\nu} = \frac{\sigma \cdot |\vec{E}|^2}{h\nu} \quad (3)$$

with P the Poynting vector in $\text{W}\cdot\text{m}^{-2}$. The next step is to inject

G_{opt} into the electrical tool to simulate the behavior of carriers in the substrate. As we want to understand the diffusion, recombination, and collection of all generated electrons, the depth in the silicon is parameterized to ensure that all the photons are absorbed ($3\mu\text{m}$ in blue, $6\mu\text{m}$ in green and $10\mu\text{m}$ in red).

B. TCAD simulations

1) Principle

We use the Synopsys Sentaurus TCAD [9] suite to firstly perform process simulations that deal with modeling the front-end-of-line (FEOL) steps in the sensor manufacturing. Then, device simulations are the electro-optical behavior of the system in operating conditions. Both simulations are required to allow the most advanced description of complex physical, optical and electrical phenomenon encountered in CMOS Image Sensors.

2) 3D Bayer modeling

The FEOL part of the 3D Bayer has been built thanks to the following methodology. We firstly perform layout based process simulations of 2D domains that are perpendicular to the pixels transfer gates: these different cuts consider topology that might significantly impact doping distribution inside the pixels such as the presence / absence of Shallow-Trench-Isolation (STI). Then, the obtained end-of-process 2D doping distributions are extruded thanks to Sentaurus Structure Editor [9] along the third dimension to fill the pixel regions. Additional extrusions of 1D end-of-process specific implants are incorporated to fill the 3D doping distribution outside the domain covered by the previous 2D cuts. This strategy based on 2D process modeling ensures an adequate level of accuracy while keeping the simulation time compatible with large design of experiments.

Once the full 3D doping distribution is generated, the structure is meshed prior to device simulations. Our meshing strategy is to concentrate the smallest elements (20nm) in the photodiode / sensing-node regions to catch the strong doping gradients. Coarser (80nm) isotropic mesh is then used for photodiode surroundings (down to $1.1\mu\text{m}$ under the surface). Another coarser mesh (160nm) is applied between $1.1\mu\text{m}$ and $3\mu\text{m}$ for 450nm , $6\mu\text{m}$ for 532nm and $8\mu\text{m}$ for 633nm simulations. Finally, the bottom of the structure has the biggest elements (900nm).

Since the previously simulated Optical Generation data field is mapped on a Lumerical mesh, we need to interpolate it on a Sentaurus grid format. This mandatory step is performed on an equivalent tensor grid thanks to a routine with a maximum interpolation error that is smaller than 0.1% . Finally, the Optical Generation data is once again interpolated on the doping dependent mesh which will be responsible for another interpolation error.

A compromise must be found between high accuracy on Optical Generation gradients, doping distribution gradients and the final number of elements to allow reasonable CPU time. Both strongest Optical Generation and doping gradients are found in the same regions – i.e. close to the Silicon surface

– therefore, a doping dependent mesh provides a satisfactory description. Our final structure has 340,000 elements (Fig. 3) and the resulting Optical Generation interpolated on device simulation mesh (from left to right: $\lambda=450\text{nm}$, $\lambda=532\text{nm}$ and $\lambda=633\text{nm}$). Half of the pixels has been blanked in the x and y directions to show light focalization inside the pixels.

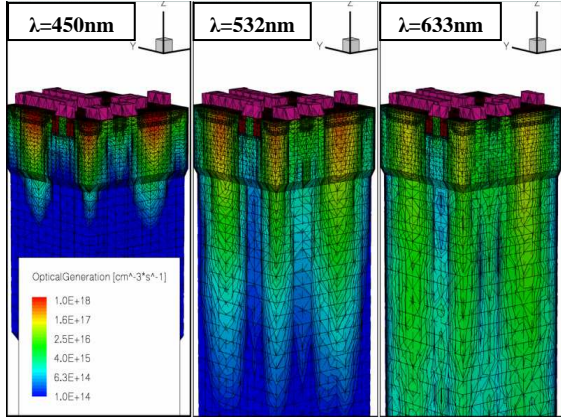


Fig. 3 3D Optical Generation in the Bayer interpolated on device simulation mesh (from left to right: $\lambda=450\text{nm}$, $\lambda=532\text{nm}$ and $\lambda=633\text{nm}$). Half of the pixels has been blanked in the x and y directions to show light focalization inside the pixels.

3) TCAD device simulation setup

Sensor device simulations have been performed thanks to Sentaurus Device tool [9] which resolves the Poisson equation and both electrons and holes continuity equations in the structure.

The Image Sensor is a periodic array of Bayer structures, therefore, the use of periodic boundary conditions in both the x and y directions is mandatory to accurately consider electrical crosstalk i.e. electrons that may flow from one pixel to all its neighbors.

As in light capture operational conditions, the device simulation experimental protocol consists of the three following steps: pixels Reset, Illumination, Readout. The Reset is performed by initializing electron Fermi level to an arbitrary high value in the pixels in order to empty all the photodiodes. Then, thermal generation of electron-hole pairs (Shockley-Read-Hall model with Scharfetter doping dependence [10-13]) fills the photodiodes by dark current. Because of the sudden character of this artificial Reset operation, we let the system go back to a linear regime by waiting for 1ms. During that time, only dark current fills the photodiodes. Light is then turned on with the Lumerical Optical Generation map in the 3D Bayer and integration is performed for $t_{int}=66.7\text{ms}$. Finally, the 3D electron density is integrated in each pixel 1ms after light is stopped to obtain the number of collected electrons. Another simulation without light is performed to obtain the number of dark current electrons to be subtracted in the final pixel quantum efficiency (QE) calculation (4):

$$QE_{pixel}(\lambda) = \frac{\int_{pixel}^{light} n \cdot d\tau - \int_{pixel}^{dark} n \cdot d\tau}{t_{int} \cdot \iint_{pixel} \Phi \cdot d\sigma} \quad (4)$$

where λ is the wavelength, n is the electron density, t_{int} is the integration time and Φ is the incident photon flux.

III. COUPLED OPTICAL/TCAD SIMULATIONS RESULTS

1) Measurements and calibration

For the calibration, we choose to limit the angular distribution of the source to limit the computation time and memory requirement. So we used plane wave for simulation and nearly collimated (f-number=200), narrow band beam for $1.75\mu\text{m}$ pixels QE characterization. The experimental setup is based on a stabilized halogen light source. The intensity is adjusted by inserting neutral density filters. The bands of interest ($450\text{nm}\pm 5\text{nm}$, $532\text{nm}\pm 5\text{nm}$, $633\text{nm}\pm 5\text{nm}$) are obtained with interference filters. The illumination is recorded in real-time by a calibrated photodiode. Sensor under test provides images under standard operating conditions. Standard pre-processing (image average, dark subtraction) is performed in order to minimize the measurement noise.

Process simulations calibration has been performed on the basis of STMicroelectronics SIMS profiles and TCAD devices simulations database. It shows a good agreement with a large number of standard electrical characteristics on various devices. Furthermore, we add a constant doping profile in a $1\mu\text{m}$ range from the surface to account for 3D effects including Well-Proximity-Effects that are not taken into account in our 2D simulations. Such effects reduce 3D photodiode extension, thus photodiode efficiency.

The coupled Optical/TCAD simulations results are hence used to compute the $QE(\lambda)$ accounting for both optical and electrical crosstalks. Following results aim at demonstrating that our coupled simulation strategy is calibrated and reproduces various BEOL and FEOL trials.

2) Bayer without color filters

Fig. 4 shows the quantum efficiency of a Bayer without color filters. Moreover, this Bayer corresponds to a specific FEOL design where voluntary different doping distributions have been realized inside each pixel. Although at 450nm all pixels behave in a similar manner, this is no longer the case at 532nm and 633nm . Indeed, Green and Red pixels catch more electrons than the Blue one because of its specific isolation scheme. The small difference between Green and Red pixels is explained by a smaller Red photodiode extension.

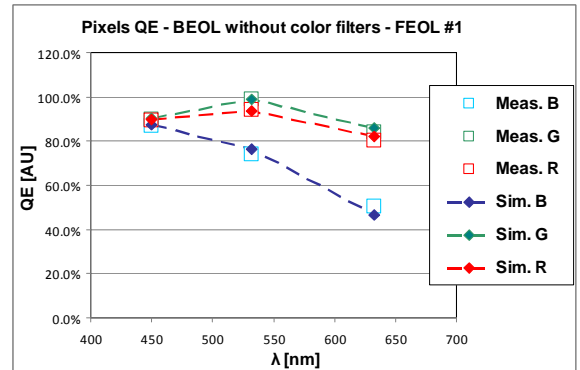


Fig. 4 Pixels $QE(\lambda)$ without color filters in the BEOL and with FEOL process #1. Scaling factors are 0.84 ($\lambda=450\text{nm}$), 0.89 ($\lambda=532\text{nm}$) and 0.88 ($\lambda=633\text{nm}$). Normalization is performed vs. Green QE at 532nm .

Note that at each wavelength, a scaling factor is applied on simulated Blue, Green and Red $QE(\lambda)$. It is calculated as the ratio between measured Bayer average $QE(\lambda)$ and simulated

Bayer raw average $QE(\lambda)$. This factor reflects imperfections that are not considered in optical simulations (like interface roughness) and is consequently wavelength dependent.

3) Bayer with color filters

Adding color filters in the BEOL strongly affects the overall Bayer response because of color filters transmission (Fig. 5). FEOL process #2 has identical doping distribution in Green and Red pixels. The strong response of Red pixel at 532nm and Green pixels at 633nm indicate the presence of crosstalk between neighboring pixels.

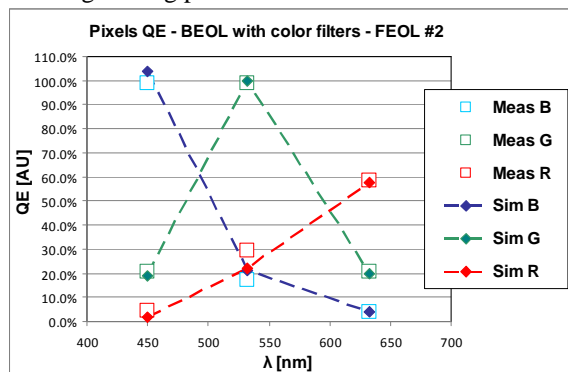


Fig. 5 Pixels $QE(\lambda)$ with color filters in the BEOL and with FEOL process #2. Scaling factors are 0.82 ($\lambda=450\text{nm}$), 0.86 ($\lambda=532\text{nm}$) and 0.69 ($\lambda=633\text{nm}$). Normalization is performed vs. Green QE at 532nm.

In order to evidence that our simulation tool well describes the evolution of electrical crosstalk with respect to various pixels doping distributions, we simulated two additional FEOL process changes that can be compared with measurements.

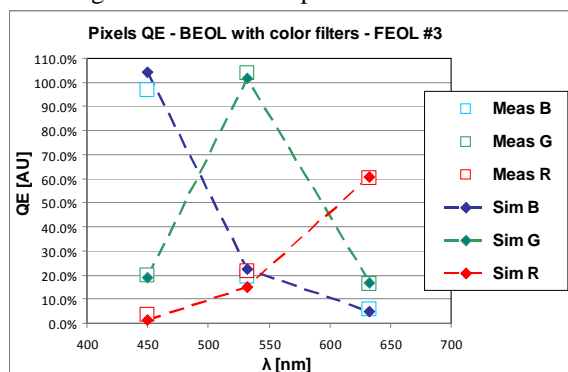


Fig. 6 Pixels $QE(\lambda)$ with color filters in the BEOL and with FEOL process #3. Scaling factors are 0.82 ($\lambda=450\text{nm}$), 0.86 ($\lambda=532\text{nm}$) and 0.69 ($\lambda=633\text{nm}$). Normalization is performed vs. Fig. 5 Green QE at 532nm.

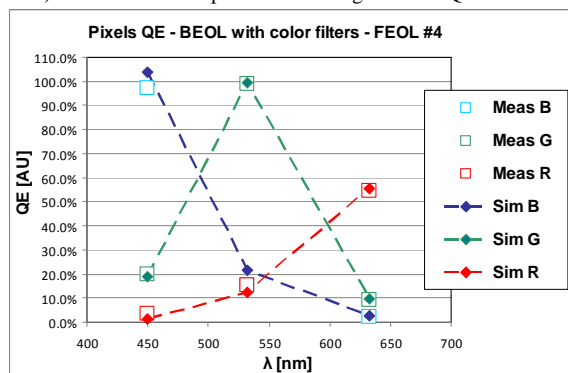


Fig. 7 Pixels $QE(\lambda)$ with color filters in the BEOL and with FEOL process #4. Scaling factors are 0.82 ($\lambda=450\text{nm}$), 0.86 ($\lambda=532\text{nm}$) and 0.69 ($\lambda=633\text{nm}$). Normalization is performed vs. Fig. 5 Green QE at 532nm.

FEOL process #3 is a slight modification of the doping concentration in depth for all pixels. Its response (Fig. 6) shows it is possible to improve Green QE while reducing Red pixel QE at 532nm by acting on electron diffusion in depth. This behavior is confirmed by the reduction of Green QE at 633nm which is well reproduced by our simulations.

Accordingly, our simulations also well predict that FEOL process #4 (Fig. 7), which adds a cut-off in depth, reduces Red QE at 633nm in particular. As expected, this also strongly reduces both 532nm and 633nm electrical crosstalks.

IV. CONCLUSION

In very small pixels, crosstalk becomes one of the main performance limiting factors, with strong 3D and neighboring effects. Moreover crosstalk arises from two distinct phenomena (optical and electrical) that are in strong interaction. Therefore, an approach that couples dedicated simulations tools is mandatory. Our strategy is thus to link Optical simulations to TCAD process and device modeling.

The present study shows the ability to describe both BEOL and FEOL process changes in agreement with sensor characterization data. Although some adjustments are required, like global optical stack transmission scaling and 3D corrections to 2D doping distributions, electro-optical performances of four different sensors can be reproduced within a few percents error.

This methodology, validated on 1.75 μm pixels, can easily be implemented on more complex Image Sensors technologies.

REFERENCES

- [1] F. Hirigoyen et al., "FDTD-based optical simulations methodology for CMOS image sensor pixels architecture and process optimization", *Proc. of SPIE IS&T Electronic Imaging*, vol. 6816-8, 2008.
- [2] K. S. Yee, "Numerical Solution of Initial Boundary Value Problems Involving Maxwell's Equations in Isotropic Media," *IEEE Trans. Antennas Propagat.*, vol. 14, no. 3, pp. 302-307, May 1966.
- [3] A. Taflov and S. C. Hagness, *Computational Electrodynamics : the finite-difference time-domain method*, 2nd ed., H. E. Schrank Series Editor, Artech House, Boston, Ma, 2000.
- [4] Lumerical Solutions, Inc. Available: <http://www.lumerical.com>.
- [5] A. Crocherie et al., "Three-dimensional broadband FDTD optical simulations of CMOS image sensor", *Proc. SPIE*, vol. 7100-103, 2008.
- [6] J. Vaillant et al., "Uniform illumination and rigorous electromagnetic simulation applied to CMOS image sensor", *Optics Express*, vol. 15, no. 9, April 2007.
- [7] M. Cohen et al., "Fully Optimized Cu based process with dedicated cavity etch for 1.75 μm and 1.45 μm pixel pitch CMOS Image Sensors", *International Electron Devices Meeting IEDM'06*, 2006.
- [8] V. S. Vavilov, "On photo-ionization by fast electrons in germanium and silicon", *J. Phys. Chem. Solids*, Pergamon Press, vol. 8, 1959.
- [9] Synopsys TCAD tools: <http://www.synopsys.com/Tools/TCAD>
- [10] D. J. Roulston, "Modeling and Measurement of Minority-Carrier Lifetime versus Doping in Diffused Layers of n+-p Silicon Diodes", *IEEE Transactions on Electron Devices*, vol. ED-29, no. 2, 1982.
- [11] J. G. Fossum, "Computer-Aided Numerical Analysis of Silicon Solar Cells", *Solid-State Electronics*, vol. 19, no. 4, 1976.
- [12] J. G. Fossum et al., "A Physical Model for the Dependence of Carrier Lifetime on Doping Density in Nondegenerate Silicon", *Solid-State Electronics*, vol. 25, no. 8, 1982.
- [13] J. G. Fossum et al., "Carrier Recombination and Lifetime in Highly Doped Silicon", *Solid-State Electronics*, vol. 26, no. 6, 1983.